23rd ABCM International Congress of Mechanical Engineering
December 6-11, 2015, Rio de Janeiro, RJ, Brazil

APPLICATION OF SHUNTED PIEZOELECTRIC MATERIALS IN AEROELASTICITY

Leandro de Souza Leão
Antônio Marcos Gonçalves de Lima
André Garcia Cunha Filho
Universidade Federal de Uberlândia (UFU)
leandro.leao.eng@gmail.com
amglima@mecanica.ufu.br
andregc@gmail.com

Maurício Vicente Donadon
Instituto Tecnológico de Aeronáutica (ITA)
donadon@ita.br

Abstract. *This paper presents a numerical study on the influence of a multimodal shunt circuit parameters in the flutter velocity of a typical section under an unsteady flow. Flutter on typical sections is a kind of self-excited oscillation which can occur due to the interaction with the airflow. In the flutter point, when the critical dynamic pressure is reached, the vibrations of the typical section become unstable and increase fast and significantly in time. As a result, it can lead the structure to failure. Thus, it becomes important to investigate the possibility of reducing the effects of flutter in order to increase the reliability of composite structures during service. In this work, the aero-electromechanical dynamic model formulation is based on the Hamilton principle. The unsteady aerodynamic forces are calculated based on the linearized thin-airfoil theory, proposed by Theodorsen. The passive element responsible for the energy dissipation is a multimodal resonant shunt circuit in series topology, attached to a piezoelectric patch. An iterative solution algorithm is proposed to solve the resultant nonlinear eigenvalue problem, based on the K-method. The optimum shunt tuning is firstly performed using Hagood and Flotow's propositions; then, it is used an heuristic optimization algorithm, based on Differential Evolution. The preliminary results indicate that the flutter speed can be affected by the passive control, both in its mechanical aspect as electrical.*

Keywords: *Aeroelasticity, flutter, piezoelectric materials, multimodal shunt circuit, passive control*

1. INTRODUCTION

Flutter is the most important aeroelastic phenomenon and consists of a dynamic self-excited instability caused by the interaction of elastic, aerodynamic and inertial forces (Pegado, 2003). It was firstly verified by Jordan, due to failures arising in V2 rocket, a supersonic german rocket, developed in the Second World War (Jordan, 1956; Filho *et al.*, 2015).

This phenomenon occurs when, due to an air flow of increasing speed, two or more natural modes coalesce themselves (join). There are two types of flutter: one that occurs in typical section, that concerns this study, and presents vibration amplitudes of exponentially growing, leading to its collapse; and the other type of flutter occurs on plates, in which due to geometric non-linearities, internal tensions arise at the panel plane, limiting the amplitudes of vibrations, thereby causing fatigue on itself or on the support structure (Dowell, 1975).

For many years, unsteady aerodynamics theories have been developed for a variety of uses (Walker, 2012). The Theodorsen (1935) theory presents a linear approach, but there are non-linear theories as well, considering airfoil non-uniform motion. Kármán and Sears (1938) derived the formulae for lift and pitching moment for a general non-uniform motion, in a non-closed form result (Walker, 2012). Partil (2003) related aeroelastic flutter with thrust generation, using energy transfer (Walker, 2012).

In this context, aerodynamic non-conservative forces are included in this study by considering an unsteady flow, which is implemented in accordance with the Linearized Thin-Airfoil Potential Theory, proposed by Theodorsen (1935). This theory is implemented on the frequency domain and assumes small perturbations and harmonic motion for the airfoil inside an inviscid fluid (Bismarck-Nasr, 1999; Benini, 2002; Walker, 2012).

The results were reached using a computer code which was constructed on discrete method and simulates, for a typical section, the aerodynamic loading, as the airflow speed increases, until the reach of flutter. This way one can compare the efficiency of the shunted passive control.

Aeroelastic stability control is performed in order to increase flutter speed on a typical section. Many kinds of passive, semi-active and active control have been addressed on typical sections, in order to increase their aeroelastic stability. Song and Li (2012); Almeida *et al.* (2012) tryed to control aeroelastic flutter, by using active control, related with piezo-electric materials. Kouchakzadeh *et al.* (2010) made a parametric study of varying in-plane forces, fiber orientation and aerodynamic damping on the aeroelastic response in flutter for laminated composite plates (Filho *et al.*, 2015).

The control strategy chosen in this work is a passive one, performed by a multimodal resonant shunt circuit, in series topology. The system is composed by a resistor and an inductor, in series with the inherent capacitance of the piezoelectric patch, composing a RLC electrical circuit. This circuit will be firstly tuned according to Hagood and Flotow (1991) equations in order to damp the lift and pitching natural modes of a typical section. In a second moment, the shunt tuning will be performed, using an heuristic algotithm of optimization, known as *Differential Evolution*, (Price and Storn, 1997; Lobato and Steffen, 2007).

A resonant shunt circuit has a similar behavior to the Dynamic Vibrations Absorber (D.V.A.), presenting even the same invariant points (Hagood and Flotow, 1991; Wu, 1998). In this passive control configuration, the resistances have the power of reducing the amplitude of the peaks, while the inductors are responsible for displacing these peaks into the frequency axis (Wu and Bicos, 1997).

The results will present the passive control efficiency under a parametric study for evaluating the influence of shunt tuning and design project of the typical section, on its aeroelastic stability.

2. THE AERO-ELECTROMECHANICAL DYNAMIC MODEL FOR THE TYPICAL SECTION

One considers a typical section coupled with the shunted piezoelectric material based multimodal shunt circuit shown in Fig. 1.

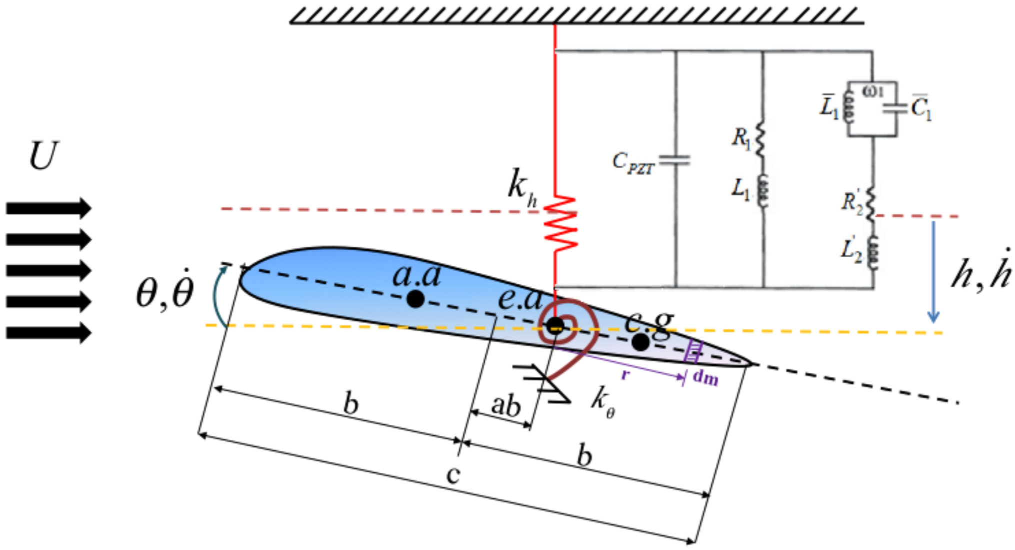

Figure 1. Typical section coupled with multimodal shunt circuit

The model has a translational spring with stiffness K_h and a torsion spring, with stiffness K_θ. These springs are attached to the airfoil at the shear center. Therefore, it is a two mechanical degrees of freedom model $\{q\}^T = \{h, \theta\}^T$. The heigth h is measured at the shear center (elastic axis). The downward displacement of any other point on the airfoil is:

$$z = h(t) + r\theta(t) \tag{1}$$

where r is a distance measured from the elastic axis ($e.a$). The other acronyms, $a.a$ and $c.g$, are the section aerodynamic and gravity centers, respectively. The 1-D constitutive equations for the piezoelectric material assuming through the thickness polarization only are given as follows:

$$D_3 = e_{31}\epsilon_1 + \xi_{33}E_3 \tag{2}$$

$$\sigma_1 = C_{11}\epsilon_1 - e_{31}\, E_3 \tag{3}$$

The aero-eletromechanical Lagrangian L for the typical section can be written as follows:

$$L = T - U \tag{4}$$

where the kinetic energy T is given by:

$$T = \frac{1}{2}\int \rho \dot{z}^2 dr = \frac{1}{2}(\dot{h}^2 \int \rho dr + 2\dot{h}\dot{\theta}\int \rho r dr + \dot{\theta}^2 \int \rho r^2 dr) \tag{5}$$

Defining the airfoil mass $m = \int \rho dr$, the second moment of inertia of the airfoil about the elastic axis $I_\theta = \int \rho r^2 dr = mr_\theta^2$ and the first moment of inertia of the airfoil about the elastic axis $S_\theta = \int \rho r dr = mr_\theta$, results in:

$$T = \frac{1}{2}(m\dot{h}^2 + 2mr_\theta \dot{h}\dot{\theta} + I_\theta \dot{\theta}^2) \tag{6}$$

The electromechanical strain energy is defined as follows:

$$U = \frac{1}{2}K_h h^2 + \frac{1}{2}K_\theta \theta^2 + \frac{1}{2}\int_{V_{pzt}} \epsilon_1 \sigma_1 dV - \frac{1}{2}\int_{V_{pzt}} D_3 E_3 dV \tag{7}$$

The substitution of the constitutive equations Eqs (2) and (3) in the eletromechanical Strain Energy U, with $\epsilon_1 = h/l_{pzt}$, where l_{pzt} is the PZT patch length results:

$$U = \frac{1}{2}(K_h + \frac{C_{11}A_{pzt}}{l_{pzt}})h^2 - \frac{e_{31}}{l_{pzt}}E_3 h V_{pzt} + \frac{1}{2}K_\theta \theta^2 - \frac{1}{2}\xi_{33}E_3^2 V_{pzt} \tag{8}$$

Assuming a constant electrical field along the thickness direction of the PZT patch, $E_3 = \frac{-\phi}{t_{pzt}}$, the internal energy can be rewritten in terms of the electrical potential ϕ as follows:

$$U = \frac{1}{2}(K_h + \frac{C_{11}A_{pzt}}{l_{pzt}})h^2 + \frac{e_{31}V_{pzt}}{t_{pzt}l_{pzt}}\phi h + \frac{1}{2}K_\theta \theta^2 - \frac{1}{2}\frac{V_{pzt}\xi_{33}}{t_{pzt}^2}\phi^2 \tag{9}$$

The Hamilton principle for the aero-electromechanical model is defined as follows:

$$\delta \int_{t_2}^{t_1} (T - U - W_h - W_\theta - W_\phi)dt = 0 \tag{10}$$

where $W_h = F_{aer}h$, $W_\theta = M_{aer}\theta$ are the work done by the nonconservative aerodynamic forces in the plunge and pitch directions, respectively and $W_\phi = Q\phi$ is the work done the electrical force, where Q is the electrical charge.

The application of the Hamilton principle results in the following system of equilibrium equations:

$$\int_{t_1}^{t_2} \left\{ \begin{array}{c} \delta h \\ \delta\theta \\ \delta\phi \end{array} \right\}^T \left\{ \left[\begin{array}{ccc} m & mr_\theta & 0 \\ mr_\theta & I_\theta & 0 \\ 0 & 0 & 0 \end{array} \right] \left\{ \begin{array}{c} \ddot{h} \\ \ddot{\theta} \\ \ddot{\phi} \end{array} \right\} + \left[\begin{array}{ccc} K_{hh} & 0 & K_{h\phi} \\ 0 & K_{\theta\theta} & 0 \\ K_{h\phi} & 0 & K_{\phi\phi} \end{array} \right] \left\{ \begin{array}{c} h \\ \theta \\ \phi \end{array} \right\} - \left\{ \begin{array}{c} F_{aer} \\ M_{aer} \\ Q \end{array} \right\} \right\} dt = 0 \tag{11}$$

where: $K_{hh} = K_h + \frac{C_{11}A_{pzt}}{l_{pzt}}$, $K_{h\phi} = \frac{-e_{31}V_{pzt}}{l_{pzt}t_{pzt}}$, $K_{\theta\theta} = K_\theta$ and $K_{\phi\phi} = \frac{V_{pzt}\xi_{33}}{t_{pzt}^2}$

After performing the Laplace transform the system of equilibrium equations can be written in the frequency domain as follows:

$$-\omega^2 \left[\begin{array}{ccc} m & mr_\theta & 0 \\ mr_\theta & I_\theta & 0 \\ 0 & 0 & 0 \end{array} \right] \left\{ \begin{array}{c} h(\omega) \\ \theta(\omega) \\ \phi(\omega) \end{array} \right\} + \left[\begin{array}{ccc} K_{hh} & 0 & K_{h\phi} \\ 0 & K_{\theta\theta} & 0 \\ K_{h\phi} & 0 & K_{\phi\phi} \end{array} \right] \left\{ \begin{array}{c} h(\omega) \\ \theta(\omega) \\ \phi(\omega) \end{array} \right\} = \left\{ \begin{array}{c} F_{aer}(\omega) \\ M_{aer}(\omega) \\ Q(\omega) \end{array} \right\} \tag{12}$$

The third equilibrium equation can be incorporated into the first one as follows:

$$K_{h\phi}h(\omega) + K_{\phi\phi}\phi(\omega) = Q(\omega) \tag{13}$$

The relationship between $Q(\omega)$ and $\phi(\omega)$ is obtained from the Ohm's law in the frequency domain:

$$Q(\omega) = \frac{Z^{-1}(\omega)L}{i\omega}\phi(\omega) \tag{14}$$

The substitution of Eq. (14) into Eq. (13) leads to the following equation:

$$\phi(\omega) = K_{h\phi}(\frac{Z^{-1}(\omega)L}{i\omega} - K_{\phi\phi})^{-1}h(\omega) \tag{15}$$

Then, substituting the Eq. (15) into the first equation of Eq. (12) reduces the system of equilibrium equations to two equations only given by:

$$-\omega^2 \begin{bmatrix} m & mr_\theta \\ mr_\theta & I_\theta \end{bmatrix} \begin{Bmatrix} h(\omega) \\ \theta(\omega) \end{Bmatrix} + \begin{bmatrix} (K_{hh} + K_{h\phi}(\frac{Z^{-1}(\omega)L}{i\omega} - K_{\phi\phi})^{-1}K_{\phi h})) & 0 \\ 0 & K_{\theta\theta} \end{bmatrix} \begin{Bmatrix} h(\omega) \\ \theta(\omega) \end{Bmatrix} = \begin{Bmatrix} F_{aer}(\omega) \\ M_{aer}(\omega) \end{Bmatrix} \tag{16}$$

where $\omega_h^2 = \frac{K_{hh}}{m}$, $\omega_\theta^2 = \frac{K_\theta}{I_\theta}$, $\bar{r}_\theta = \frac{r_\theta}{b}$, $\omega_{h\phi}^2 = \frac{K_{\phi h}(\frac{Z^{-1}(\omega)L}{i\omega} - K_{\phi\phi})^{-1}K_{\phi h}}{m}$

Eq. (16) reads,

$$-\omega^2 \begin{bmatrix} 1 & \bar{r}_\theta \\ \bar{r}_\theta & \bar{r}_\theta^2 \end{bmatrix} \begin{Bmatrix} h(\omega)/b \\ \theta(\omega) \end{Bmatrix} + \begin{bmatrix} (\omega_h^2 + \omega_{h\phi}^2) & 0 \\ 0 & \omega_\theta^2\bar{r}_\theta^2 \end{bmatrix} \begin{Bmatrix} h(\omega)/b \\ \theta(\omega) \end{Bmatrix} = \begin{Bmatrix} \frac{F_{aer}(\omega)}{mb} \\ \frac{M_{aer}(\omega)}{mb^2} \end{Bmatrix} \tag{17}$$

2.1 Aerodynamic loads

According to Theodorsen's theory, the unsteady aerodynamic force and moment on the frequency domain are respectively given as follows:

$$F_{aer}(\omega) = \pi\rho b^3\omega^2[\frac{h}{b}L_h + \theta(L_\theta - (0.5 + a)L_h)] \tag{18}$$

$$M_{aer}(\omega) = \pi\rho b^4\omega^2 \left[\{M_h - (0.5 + a)L_h\}\frac{h}{b} + \left\{M_\theta - (0.5 + a)(L_\theta + M_h) + (0.5 + a)^2\right\} L_h\right] \tag{19}$$

where $L_h = 1 - i2C\frac{1}{k}$, $L_\theta = \frac{1}{2} - i\frac{1+2C}{k} - \frac{2C}{k}^2$, $M_h = \frac{1}{2}$, $M_\theta = \frac{3}{8} - i\frac{1}{k}$

The Theodorsen function C is defined in terms of reduced frequency $k = \omega b/V$, letting V be the airflow speed.

$$C(k) = 0.5 + \frac{0.0075}{ik + 0.0455} + \frac{0.10055}{ik + 0.3} \tag{20}$$

For quasi-steady aerodynamics the Theordorsen function is independent on the frequency and is reduced to:

$$C(k) = 1.0 \tag{21}$$

2.2 Resultant nonlinear eigenvalue problem

The substitution of the aerodynamic force and moment into Eq. (17) leads to the following set of nonlinear system of equations:

$$-\Omega^2 \begin{bmatrix} 1 & \bar{r}_\theta \\ \bar{r}_\theta & \bar{r}_\theta^2 \end{bmatrix} \begin{Bmatrix} h(\omega)/b \\ \theta(\omega) \end{Bmatrix} + \begin{bmatrix} (R_{h\theta}^2 + R_{h\phi}^2) & 0 \\ 0 & \bar{r}_\theta^2 \end{bmatrix} \begin{Bmatrix} h(\omega)/b \\ \theta(\omega) \end{Bmatrix} = \frac{\Omega^2}{\mu}[A] \tag{22}$$

where $[A]$ is the aerodynamic matrix given by:

$$[A] = \begin{bmatrix} L_h & L_\theta - (0.5+a)L_h \\ M_h - (0.5+a)L_h & M_\theta - (0.5+a)(L_\theta + M_h) + (0.5+a)^2 L_h \end{bmatrix} \tag{23}$$

and the mass ratio is defined as $\mu = m/\pi\rho b^2 L$, letting m be the airfoil mass per unit of length, L.

Defining $\Omega^2 = \omega^2/\omega_\theta^2$, $R_{h\theta}^2 = \omega_h^2/\omega_\theta^2$ and $R_{h\phi}^2 = \omega_{h\phi}^2/\omega_\theta^2$. The nonlinear eigenproblem can be written in a compact form as follows:

$$\{[K(\omega)] - \Omega^2\{[M] + \frac{1}{\mu}[A(\omega)]\}\}\{q(\omega)\} = \{0\} \tag{24}$$

2.3 Determination of the optimum shunt circuit parameters

The determination of the multimodal shunt circuit parameters is based on the work proposed by Hagood and Flotow (1991). According to these authors the optimum resistance and inductance for the ressonant shunt circuit in series are given by:

$$R_n = \frac{\sqrt{2}K_{31}}{C_{PZT}\omega_n(1+K_{31}^2)} \tag{25}$$

$$L_n = \frac{1}{C_{PZT}\omega_n^2(1+K_{31}^2)} \tag{26}$$

where n=1,2 (bi-modal shunt circuit); K_{31} is the material electromechanical coupling factor and $C_{PZT} = \xi_{33}(b_{pzt}L_{pzt})/t_{pzt}$ is the static capacitance of the PZT patch.

After that, the *Differential Evolution* algorithm uses these values of resistance and indctance as initial points, for calculating new optimized values, that will be used for a new shunt tuning.
Both results of tuning by Hagood and Flotow or by this algorithm will be showed in the section *Numerical Simulations*.

3. SOLUTION ALGORITHM FOR SOLVING THE NONLINEAR EIGENVALUE PROBLEM

The solution method proposed here to solve the nonlinear eigenvalue problem given by Eq. (24) is based on the iterative procedure shown in Fig.2 combined with V-g method for flutter velocity determination (Nam and Kim, 2001).

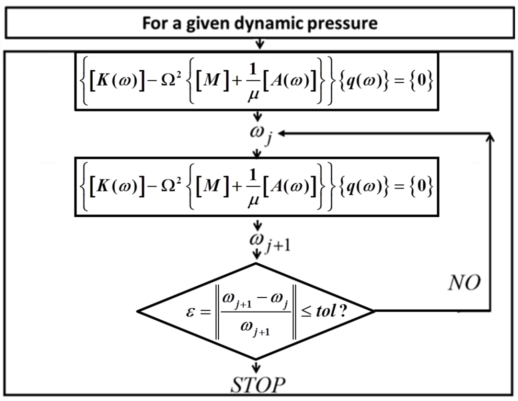

Figure 2. Iterative solution method

Initially, one adopts a constant value of natural frequency ω_j, that will feed the eq. 24. The result of this equation of motion, in that adopted frequency, will generate a new value of natural frequency ω_{j+1}, that will feed back, in the next iteration, the same equation. Each calculated value of frequency (ω_{j+1}), will be compared with the last iteration's frequency, that generated it (ω_j). This procedure continues, untill the difference between these two frequencies becomes smaller than a determined tolerence. This procedure will be repeated for each value of dynamic pressure.

4. NUMERICAL SIMULATIONS

Numerical simulations were carried out in order to investigate the influence under flutter speed of:

- typical section geometry;
- electrical shunt parameters.

There is a big influence of geometrical parameters under flutter speed. There is even the possibility of designing a typical section that never suffers flutter only by choosing the correct emplacement of its elastic axis, aeroelastic axis and gravity center(Bismarck-Nasr, 1999). For this purpose, it will be performed a parametric study of some geometrical parameters of a typical section, which can help increasing flutter speed.

Also, some parameters of the multimodal resonant shunt circuit will be compared, in order to measure its contribution for the efficiency of the final passive control. On this study it will be presented the mechanical stiffness influence of the piezoelectric patch on flutter speed. Also the tuning influence will be analyzed, by comparing Hagood and Flotow's with the optimized values, found using *Differential Evolution*.

4.1 Initial Configuration

All the performed tests, will be compared with an initial configuration which presents a gain of 6,87% on flutter speed due to the passive control. This configuration uses a multimodal resonant shunt circuit in series topology, which was firstly tuned using Hagood and Flotow's equations and uses a piezoelectric patch of type G1195, according to Table 2. The parameters of the typical section for this initial condition are listed in Table 1.

Table 1. Typical section parameters

Typical section parameters	
$\bar{r}_\theta$	0.3
$\omega_h(rad/s)$	300
$\omega_\theta(rad/s)$	300
ρ_{air} (kg/m^3)	1.225
ab (m)	-0.075
b (m)	0.5

Table 2. Eletromechanical properties for the G1195 PZT patch

G1195 PZT patch	
$C_{11}(GPa)$	69
ρ (kg/m^3)	7700
e_{31} (C/m^2)	18.1
ξ_{33} (F/m)	1.6e^{-6}
d_{31} (N/mV)	2.68e^{-9}

The results for this initial configuration are shown in Figure 1. According to the figure, one can notice that the passive control increases flutter speed from 197,058 m/s to 210,595 m/s, a gain of 6,87%. These results use non-stationary aerodynamics and will be the base for comparison of the parameters discussed above.

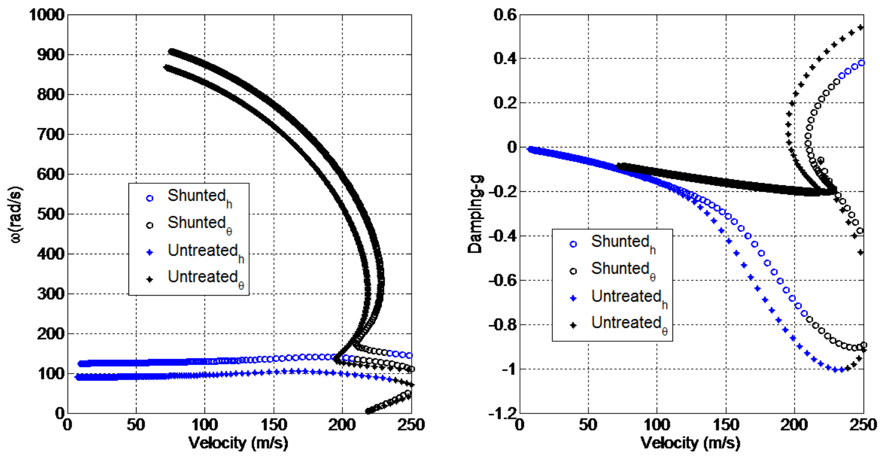

Figure 3. Gain of 6,87% for initial configuration

4.2 Influence of the typical section geometry

4.2.1 Semi-chord (b)

The smaller the semi-chord, the bigger the gain noticed. But the semi-chord shouldn't be very small for avoiding discontinuities on the V-g diagram. Also, when increasing the value of this parameter, flutter speed increases for both untreated and shunted structure. The results will be presented in a table for better visualization.

Table 3. Influence of the $semi-chord(b)$

Semi-chord $b(m)$	Untreated $V_{flutter}(m/s)$	Shunted $V_{flutter}(m/s)$	Gain (%)
$b < 0,25$	discontinuities	discontinuities	discontinuities
0,25	98,529	107,772	9,38
0,50 (initial)	***197,058***	***210,595***	***6,87***
0,75	295.588	313.966	6,22
1.00	394.117	417.825	6,02

4.2.2 Distance from the elastic-axis to the center of the typical section (ab)

As the parameter ab decreases, the gain increases, until it stabilizes around the value of 7,1%. The global flutter speed is low affected, on the opposite direction of the gain.

Table 4. Influence of the parameter ab

Distance $ab(m)$	Untreated $V_{flutter}(m/s)$	Shunted $V_{flutter}(m/s)$	Gain (%)
-0,006125	193,003	206,780	7,14
-0,0125	193,341	207,114	7,12
-0,0250	194,105	207,793	7,05
-0,750 (initial)	***197,058***	***210,595***	***6,87***
-0,150	201,606	214,282	6,29

4.2.3 Mass ratio (μ)

The gain in flutter speed has a parabolic behavior in function of the mass ratio. The maximum value of gain in this case is for the initial configuration. The global flutter speed increases when increasing the mass ratio.

Table 5. Influence of the $mass\ ratio\ \mu$

Mass ratio $\mu_{(dimensionless)}$	Untreated $V_{flutter}(m/s)$	Shunted $V_{flutter}(m/s)$	Gain (%)
5	diverges	diverges	diverges
10	153,392	163,888	6,84
20 (initial)	***197,058***	***210,595***	***6,87***
30	228,170	242,256	6,17
40	253,839	268,314	5,70

4.3 Influence of Passive Control Parameters

4.3.1 Mechanical Influence of the Piezoelectric Patch

It was noticed that the biggest part of the gain in flutter speed, achieved by the passive control, was due to the mechanical stiffness of the piezoelectric patch, which was considered the same as the translation spring.

Typical Section	$V_{flutter}(m/s)$	Gain (%)
Without piezoelectric patch	197,058	5,75
Only mechanical presence of piezoelectric patch (Open Circuit)	208,388	

The table indicates that, under a total gain of 6,87%, from the initial configuration, 5,75% of it is due only to the mechanical gain, for increasing the translational stiffness when attaching the piezoelectric patch in the typical section.

4.3.2 Shunt tuning

In this section it was compared the shunt tuning influence on flutter speed. Tuning a multimodal resonant shunt circuit means to find the correct values of resistances and inductances for increasing efficiency of the passive control.

The first line indicates that, due only to the shunt presence, tuned by Hagood and Flotow, one notices a small increase in flutter speed. It means, a gain of 1,12%, because as it was said before, a gain of 5,75% was already noticed due to its mechanical presence. The total gain sums 6,87%.

The second line presents the results achieved by using the heuristic method of optimization, called *Differential Evolution*. Within this method it was possible to gain 1,07% more than tuning according to Hagood and Flotow's propositions, it means, a total gain of 7,94%.

For both Hagood and Flotow and Differential Evolution results, it is necessary to use synthetic inductors for reaching the demanded values of inductance, what will not represent a difficulty. The resistance values were found inside the standard values.

If one considers the constraints of only standard values for the resistances $(1 \rightarrow 9 \times 10^0, 10^3, 10^6)$ and the inductances $(1 \rightarrow 9 \times 10^{-6}, 10^{-3}, 10^0)$, neither tuning by Hagood and Flotow or by *Differential Evolution* algorithm does not present any gain.

Resonant shunt tuning				Untreated $V_{flutter}(m/s)$	Shunted $V_{flutter}(m/s)$	Gain $(\%)$
R1 (Ω)	R2 (Ω)	L1 (H)	L2 (H)			
1.883,6	1.317,9	17,9	8,8	197,058	210,595	6,87
789,8	1.704,9	22,2	25,6	197,058	212,706	7,94

5. CONCLUSIONS

A small increase on the aeroelastic stability may be achieved by using a multimodal resonant shunt circuit in series topology. In fact, the biggest contribution is due to the mechanical stiffness of the piezoelectric patch. The portion of the gain in flutter speed due only to the electrical control has its maximum around 2%, which was obtained by optimization. The tuning proposed by Hagood and Flotow (1991), present a gain of only 1% on aeroelastic stability.

It was observed a strong relation between the mechanical stiffness of the translation and rotation springs and the aeroelastic stability of the typical section. As the gain for the mechanical contribution is much bigger, the passive control by resonant shunt circuits should represent an alternative, that could be helpful when it is not possible to increase those values of mechanical stiffness.

The mechanical stiffness of the piezoelectric patch was considered the same as the translation spring stiffness. This was done only for equivalence and for not reaching large values of speed. If one prefers to calculate the mechanical stiffness of the piezoelectric patch, its geometry gets a big importance under flutter speed, since it changes directly the values of stiffness.

The geometry of the typical section also has a contribution on the aeroelastic stability. However, it is a question of project and not a question of efficiency of the passive control. It was verified that for smaller semi-chords, smaller values of the distance ab from the elastic axis to the center of the typical section, the bigger is the gain in flutter speed. The familiarity with the influence of the geometric project under aeroelastic stability of the typical section is also very important for guaranteeing the required behavior.

The aeroelastic analysis was performed in such a way that its equations of forces and moments could be integrated to the structural motion equations and were fitted to the computational form according to the requirements presented by Nam and Kim (2001). The aerodynamic forces and moments, for the unsteady model where formulated in the frequency domain because the interest was to predict the critical point of the flutter instability and compare the untreated and shunted typical sections.

Also, it is known that using stationary or non-stationary aerodynamic forces does not affect the prediction of flutter speed, as remarked by Bismarck-Nasr [3], since in the critical point the motion performed by the typical section presents a simple harmonic characteristic.

Acknowledgements

The authors acknowledge the financial support received for this work from CNPq, CAPES, FAPEMIG and FAPESP.

6. REFERENCES

Almeida, A., Donadon, M.V. and Almeida, S., 2012. "The effect of piezoelectric induced stress stiffening on the aeroelastic stability of curved composite panel".
Benini, G.R., 2002. "Modelo numérico para simulação da resposta aeroelástica de asas fixas".

Bismarck-Nasr, M.N., 1999. “Structural dynamics in aeronautical engineering”. In *AIAA Education Series*.

Dowell, E., 1975. *Aeroelasticity of plates and shells*.

Filho, A.G.C., Leão, L.S., de Lima, A.M.G. and Donadon, M.V., 2015. “The influence of viscoelastic damping on the aeroelastic stability of plates”. In *Proceedings of the International Conference of Structural Engineering Dynamics - ICEDyn 2015*.

Hagood, N.W. and Flotow, A.H.V., 1991. “Damping of structural vibrations with piezoelectric materials and passive electrical networks”. *Journal of Sound and Vibration*, Vol. 146, pp. 243–268.

Jordan, P.F., 1956. “The physical nature of panel flutter”.

Kouchakzadeh, M., Rasekh, M. and Haddadpour, H., 2010. “Panel flutter analysis of general laminated composite plates”. Vol. 92, pp. 2906–2915.

Kármán, V. and Sears, W.R., 1938. “Airfoil theory for non-uniform motion”. Vol. 5, No. 10, pp. 379–390.

Lobato, F. and Steffen, V.J., 2007. “Engineering system desing with multi-objective differential evolution”. In *Proceedings of the 19th International Congress of Mechanical Engineering - COBEM*.

Nam, C. and Kim, Y., 2001. *Computational Aids in Aeroelasticity Analysis using Matlab*. Taylor and Francis, 2nd edition.

Partil, M.J., 2003. “From fluttering wings to flapping flight: The energy connection”. Vol. 40, No. 2, pp. 270–276.

Pegado, H.A., 2003. *Método de Perturbações no Estudo de Não-linearidades na Aeroelasticidade de Painéis em Regime Supersônico*. Ph.D. thesis, Instituto Tecnológido de Aeronáutica.

Price, K. and Storn, R., 1997. “Differential evolution - a simple evolution strategy for fast optimization”. Vol. 22, No. 4, pp. 18–24.

Song, Z.G. and Li, F.M., 2012. “Active aeroelastic flutter alaysis and vibration control of supersonic composite laminated pate”. Vol. 94, pp. 702–713.

Theodorsen, T., 1935. “General theory of aerodynamic instability and the mechanism of flutter.” *NACA Report*.

Walker, W.P., 2012. *Optimization of Harmonically Deforming Thin Airfoil and Membrane Wings for Optimum Thurst and Efficiency*. Ph.D. thesis, Virginia Polytechnic Institute.

Wu, S.Y., 1998. “Method for multiple mode shunt damping of structural vibration using a single pzt transducer”.

Wu, S.Y. and Bicos, A.S., 1997. “Structural vibration damping experiments using improved piezoelectric shunts”. Vol. 3045.

7. RESPONSIBILITY NOTICE

The following text, properly adapted to the number of authors, must be included in the last section of the paper: The author(s) is (are) the only responsible for the printed material included in this paper.